Geomaterials (Sedimentology)

Identification of a Sturtian cap carbonate in the Neoproterozoic Sete Lagoas carbonate platform, Bambuí Group, Brazil

Lucieth Cruz Vieira [a,*], Ricardo I.F. Trindade [a], Afonso C.R. Nogueira [b], Magali Ader [c]

[a] *Departamento de Geofísica, Instituto de Astronomia, Geofísica e Ciências Atmosféricas, Universidade de São Paulo, Rua do Matão 1226, São Paulo,05508–090, SP, Brazil*
[b] *Departamento de Geociências, Universidade Federal do Amazonas. Avenida Gal. Rodrigo Ramos 3000, Manaus, 69077-000, AM, Brazil*
[c] *Équipe de physico-chimie des fluides géologiques, institut de physique du Globe de Paris, 2, place Jussieu, 75251 Paris cedex 05, France*

Abstract

A sedimentological and C–O isotopic study has been carried out in nine sections of the Sete Lagoas Formation at its classical outcropping area, in the southern tip of the São Francisco craton (central Brazil), with the objective of refining its stratigraphic position within the Neoproterozoic. At the study area, the Neoproterozoic Sete Lagoas Formation comprises two shallowing-upward megacycles, corresponding to more than 200 m in thickness. Each cycle is limited by a flooding surface amalgamated with a third-order sequence boundary. The first megacycle presents deep-platform deposits with abundance of crystal fans (aragonite pseudomorphs). These deposits are characterized by negative C-isotope values (–4.5‰). They grade upward to storm-wave and tide-influenced layers with $\delta^{13}C$ values around 0‰. In the second megacycle, a new transgression drowned the platform, depositing a thick, mixed sub-storm wave-base succession. This megacycle comprises deposits of lime mudstone-pelite rhythmite, which grade to crystalline limestone rich in organic matter, both with unusually positive $\delta^{13}C$ values (up to + 14‰). Regional correlation of Sete Lagoas deposits indicate that they rest atop glaciomarine rocks of the Macaúbas Group and basal strata show seafloor precipitates with negative $\delta^{13}C$ values. Therefore, it is possible to characterize the Sete Lagoas carbonate as a cap carbonate sequence. The very high $\delta^{13}C$ in the second megacycle together with geochronologic data suggest that this unit correlates better with post-Sturtian sequences. Some differences in the depositional record are observed between Sete Lagoas and the other post-Sturtian units previously described in North America, Australia, and Namibia. Those differences may in part be due to deposition in shallower settings of the Sete Lagoas carbonates, thus preserving a thick record of storm- and wave-influenced sedimentation not found elsewhere. Alternatively, they may also be attributed to diachronic deposition of the so-called post-Sturtian cap carbonate sequences. *To cite this article: L.C. Vieira et al., C. R. Geoscience 339 (2007).*

Résumé

Identification d'un *cap carbonate* sturtien dans la plate-forme carbonatée néoprotérozoïque de Sete Lagoas, groupe Bambuí, Brésil. Afin de préciser la position stratigraphique de la formation de Sete Lagoas dans le Néoprotérozoïque, nous avons mené une étude sédimentologique et isotopique (carbone et oxygène) de neuf sections, dans le secteur d'affleurement classique, à

* Corresponding author.
 E-mail address: lucieth@iag.usp.br (L.C. Vieira).

l'extrémité méridionale du craton de São Francisco (Brésil central). Dans ce secteur, la formation de Sete Lagoas comporte deux mégacycles régressifs, correspondant à plus de 200 m d'épaisseur. Chaque cycle est limité par une surface d'inondation confondue avec une limite de séquence de troisième ordre. Le premier mégacycle commence par des dépôts de plate-forme profonde, caractérisés par des valeurs de δ^{13}C négatives (–4,5 ‰), qui contiennent de nombreux éventails de cristaux (pseudomorphes d'aragonite). Leur succèdent des niveaux moins profonds, influencés par les marées et tempêtes, caractérisés par des valeurs de δ^{13}C voisines de 0 ‰. Au cours du second mégacycle, une nouvelle transgression ennoie la plate-forme, et une épaisse succession se dépose à la limite d'action des vagues de tempêtes. Ce mégacycle contient des rythmites de carbonates micritiques et de pélites, qui évoluent vers des carbonates cristallins riches en matière organique, et présentent des valeurs de δ^{13}C exceptionnellement positives (jusqu'à +14 ‰). Sur la base de corrélations stratigraphiques régionales, qui suggèrent que la formation de Sete Lagoas succède aux roches glaciomarines du groupe Macaúbas, ainsi que sur la base des valeurs négatives de δ^{13}C dans ses niveaux de base contenant les précipités sur le plancher sous-marin, on peut assimiler les carbonates de la formation de Sete Lagoas à une séquence de *cap carbonate*. Les valeurs de δ^{13}C, très positives, du deuxième mégacycle, ainsi que les données géochronologiques suggèrent que la formation de Sete Lagoas est post-sturtienne plutôt que post-marinoenne. Les conditions de dépôt présentent des différences notables avec celles des unités post-sturtiennes décrites en Amérique du Nord, en Australie et en Namibie. Cela peut s'interpréter, soit par un diachronisme des *cap carbonates* post-sturtiens, soit par une sédimentation dans un contexte moins profond, ayant permis ici l'accumulation d'une épaisse série dans la zone d'action des vagues de tempête. ***Pour citer cet article : L.C. Vieira et al., C. R. Geoscience 339 (2007).***

1. Introduction

The end of the Precambrian Eon is punctuated by glacial events rapidly followed by widespread carbonate sedimentation (cap carbonates), marking severe climatic changes that could have been the evolutionary bottle-necks for the Cambrian 'life-explosion' (see review in [32]). Palaeomagnetic data from Neoproterozoic glacial rocks show that ice caps have extended into equatorial latitudes by that time, implying that these ice-ages were the most extreme in Earth history [21] (see also [61] in this volume). Cap carbonates may give us an insight into the environmental changes in the aftermath of Neoproterozoic glaciations. They form transgressive sequences associated with the post-glacial sea-level rise, most of them comprising a basal carbonate unit with negative C-isotope values [41]. Anomalous structures are usually found within the first metres of the cap carbonate sequence, including tubes, stromatolitic lamination, and pseudo-tepees associated with shallow platform deposits, as well as deep-water seafloor precipitates, represented by cement-crusts and aragonite-pseudomorph crystal fans [2,25,32,36,41,43, 56,60]. Complete descriptions of cap carbonates, including stratigraphy, sedimentology, and isotopes, have recently been given for Australia, Namibia, northwestern Canada, southern China, Svalbard, and Amazonia [26,33,36,37,41,53,54]. For the Neoproterozoic, because of the scarcity of the fossiliferous record,

the variations of δ^{13}C have been often used as a tool to infer intrabasinal or even global correlations [14,26,44].

In central Brazil, carbonates of the Bambuí Group have long been reported capping glacial rocks of the Macaúbas Group and the Jequitaí Formation [16,19]. Yet, despite a number of isotopic studies performed in these units since the late 1970s [4,6,8,34,51,56,57], facies analysis and detailed stratigraphy of the carbonate succession are still lacking. Here we present a detailed description of the sedimentology and stratigraphy of the basal unit of the Bambuí Group (Sete Lagoas Formation), coupled with a C and O isotopic study on nine sections located at the classical outcropping area of this unit, around the cities of Sete Lagoas and Vespasiano, Minas Gerais State, Brazil (Fig. 1). This coupled study allowed the identification of a cap carbonate overlying the glacial rocks and its possible correlation with Sturtian cap carbonates of other Neoproterozoic sections.

2. Geological setting

The São Francisco basin covers more than 300,000 km^2 of the São Francisco craton. It comprises a basal glacial unit (Carrancas/Macaúbas/Jequitaí) covered by a thick carbonate succession (Bambuí Group) [19,38,50,62]. The basal glacial unit comprises diamictites, clast-supported conglomerates, massive sandstones, and mudstone-siltstone rhythmites deposited in
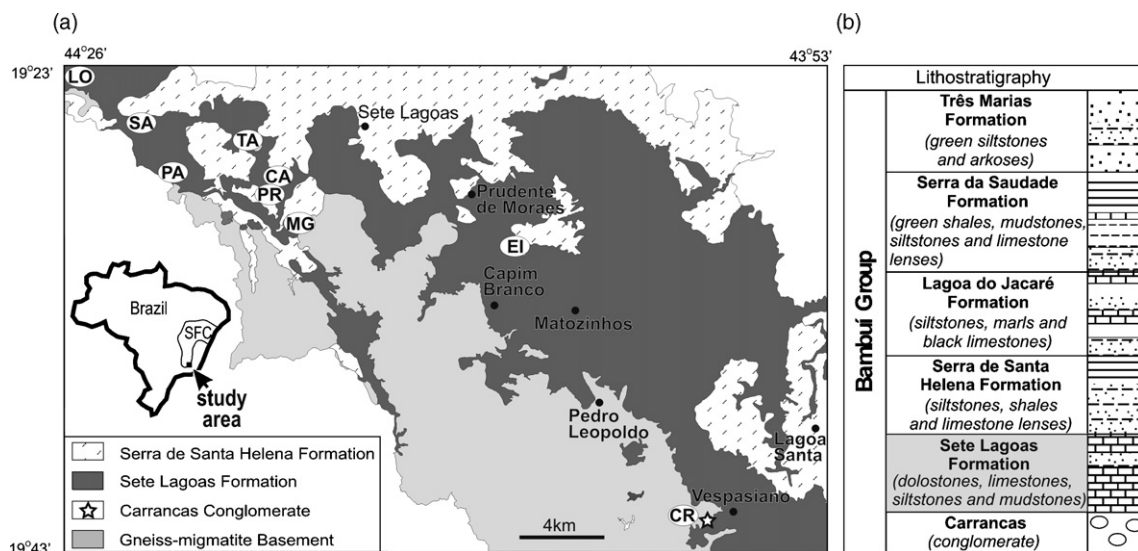
Fig. 1. (a) Geological map with location of studied sections: CR, Carrancas; CA, Canaã quarry; SA, Sambra quarry; PA, Paraíso quarry; TA, Tatiana quarry; MG, Mata Grande quarry; PR, Polícia Rodoviária; CE, Cauê quarry. (b) Lithostratigraphy of the Bambuí Group.

Fig. 1. (a) Contexte géologique et localisation des sections étudiées : CR, Carrancas ; CA, Canaã ; SA, Sambra ; PA, Paraíso ; TA, Tatiana ; MG, Mata Grande ; PR, Polícia Rodoviária ; CE, Cauê. (b) Litostratigraphie du groupe Bambuí.

a glaciomarine environment (Jequitaí) and reworked by gravity flows (Macaúbas); the Carrancas conglomerate corresponds to a lens of polymictic conglomerate with a carbonate matrix, outcropping between Palaeoproterozoic gneisses and carbonates of the Bambuí Group, and it has been interpreted as glacial in origin [50]. The Bambuí Group was divided into five units following the scheme presented in Fig. 1. The Sete Lagoas Formation is composed of dolostones, limestones, siltstones, and mudstones, with well-preserved stromatolites. The Serra de Santa Helena Formation is formed by shales and siltstones; it separates the two main carbonate units of the Bambuí Group. Siltstones, marls, and black limestones of the Lagoa do Jacaré Formation cover the pelites of the Serra de Santa Helena Formation. The Serra da Saudade includes green shales, mudstones, siltstones, and limestone lenses. These four units form two cycles of carbonate and pelitic-psammitic sedimentation. The Três Marias Formation occupies the top of the succession and comprises green siltstones and arkoses deposited in alluvial to shallow-marine environment in the foreland of Brasiliano fold belts [49]. This succession is affected by moderate to weak deformation, as a result of far-field response to the tectonic activity along the encircling Brasiliano fold belts [10].

A maximum sedimentation age of ca. 950 Ma for the rocks of the Macaúbas Group is given by U–Pb SHRIMP ages of detrital zircons from the glacial deposits [55]. Similar ages were obtained for a dike

(U–Pb in zircon and badeleyte) that cuts across the Mesoproterozoic Espinhaço Supergroup, but does not intrude on the glacial sediments [47]. Several attempts to date directly the Bambuí Group by Pb–Pb and U–Pb methods have been unsuccessful. Most ages range from 550 to 500 Ma, being coeval or even younger than the peak of tectonic activity that affects the carbonate rocks [1,6,18]. Only two ^{207}Pb–^{206}Pb isochron ages, obtained from the Sete Lagoas Formation, are older than 600 Ma and may thus represent the time of deposition. An age of 686 ± 69 Ma was obtained by Babinski et al. [6], giving a minimum depositional age for the carbonates. Another date of 740 ± 22 Ma was recently obtained by Babinski and Kaufman [5] on well-preserved cap carbonates from the southern part of the basin (our section SA, Fig. 1). The last date is the best direct age constraint on the deposition of these rocks. It falls close to the ages classically attributed to the Sturtian glacial interval [22].

3. Lithofacies and facies associations (FA)

Outcrop-based facies analysis, complemented by petrographic description of representative samples, were performed at nine sections that correspond to quarries located close to the Sete Lagoas city and to the road-outcrop of Carrancas located 15 km southeastward, close to the Vespasiano city (Fig. 1). These sections were measured and sampled for C and O isotopic analysis. From west to east, they are: Lontra

(LO), Sambra (SA), Paraíso (PA), Tatiana (TA), Polícia Rodoviária (PR), Canaã (CA), Mata Grande (MG), Cauê (CE), and Carrancas (CR). These sections show parts of the carbonates and pelites of the Sete Lagoas Formation, whereas the underlying conglomerates of the Carrancas unit crop out only in the CR section. The whole succession is covered by siltstones and sandstones of the Serra de Santa Helena Formation. In section LO, the Serra de Santa Helena formation is composed of siltstones covered by sandstone beds. In the PR and MG sections, this unit forms metric tabular layers of olive-green massive siltstones, and subordinately carbonate lenses as well as fine-grained sandstones, probably deposited in a deep-platform environment. In section MG, the basal contact of the Serra de Santa Helena Formation is brecciated.

Most sections show only weak deformation and stratigraphic relations between facies were not obliterated by tectonic imprints. When deformation is observed, it is usually concentrated at the pelitic layers interbedded with the carbonate rocks. The most deformed layers exhibit thin, flat-lying mylonitic bands associated with east-trending stretching lineation. Kinematic criteria, such as mica-fish and S–C relations, indicate top-to-the-west transport.

We have defined 13 facies based on their textural, compositional, and sedimentary structures (Table 1). We note, however, that for some facies, primary textures have been obliterated by neomorphism and/or dolomitization. Actually, fine-grained limestones presently show a microspar texture, which is interpreted to be originally micritic. On the other hand, crystalline limestone is interpreted to be originally coarse-grained, as also indicated by the presence of sparse terrigenous grains and phantom peloidal fabric in these rocks. The different facies were grouped into seven facies associations (FA), according to their palaeoenvironmental significance within the Sete Lagoas carbonate platform. These include: Carrancas conglomerate (FA1), CaCO$_3$ oversaturated outer ramp (FA2), storm-dominated middle ramp (FA3), tidal-dominated inner ramp (FA4), mixed carbonate-siliciclastic outer ramp (FA5), wave-influenced inner ramp (FA6), steepened outer ramp (FA7).

3.1. Carrancas conglomerate (FA1)

The Carrancas conglomerate, also called Carrancas diamictite, is found in section CR. It is the lowermost unit in the study area (Fig. 1) and is preserved in isolated channels incised in the Palaeoproterozoic basement. Composed of normally grading polymictic conglom-

erates (Cm facies) interbedded with pebbly sandstone lens with incipient parallel lamination (SMp facies), it defines a metre-scale finning-upward cycle, possibly of coastal to alluvial origin.

It consists of coarse-grained rounded pebbles of carbonate, granite, and quartz composition fragments, within a micrite to microsparite matrix with sparse sand-sized grains of quartz, plagioclase, biotite, and granitic lithoclasts (Fig. 2A). Under the microscope, secondary carbonates are observed in microveins cutting across the clasts or in plagioclase (saussuritisation). The textural similarity of these secondary carbonates with the matrix casts doubts on the primary origin of the carbonatic matrix of the Carrancas conglomerate. Contrasting to previous reports [19,50], no clear evidence of glacial influence could be found in these deposits during the course of this study.

3.2. CaCO$_3$ oversaturated outer ramp (FA2)

Outer ramp deposits are found at sections CR, SA and TA, implying a regional-scale lateral extension (Fig. 1). They form tabular layers up to 30 m thick, organized in centimetre-scale cycles of lime mudstone (Mp) and calcite crystal-fans (Mc), interpreted as aragonite pseudomorphs (Figs. 2B and C). The abundance of crystal-fans is the most striking feature of the Sete Lagoas carbonate succession. Aragonite-pseudomorph crystals are black to dark grey. They show acicular morphology with straight terminations, forming bottom-nucleated, upward-radiating fans up to 15 cm tall, laterally connected to thin, millimetric cement-crusts (Fig. 2C). Crystal layers are covered by light-grey or red lime mudstones showing parallel to undulating lamination reflecting the irregular surface at the top of underlying crystals, which is often truncated by stylolites. The morphology of the fans and the fact that micritic layers often onlap crystal fans indicate that these features are primary, and not a diagenetic imprint. At some places, however, blades of crystal overgrowth intersect the upper layers of aragonite pseudomorph, truncating the lamination of the upper lime mudstone beds. These overgrowths are interpreted as a diagenetic modification. In outcrop, these overgrowths are highlighted by their white-to-red colour (arrow in Fig. 2D). Occasionally, deformational features are observed in the crystal beds, such as synsedimentary faults that displace lime mudstone/cementstone cycles for some centimetres (arrow in Fig. 2B), and crystal bends toward the west. The upward decrease in frequency of crystal fans in both TA and SA sections is accompanied by the replacement of micrites of the Mp facies by terrigenous

Table 1

Summary of the carbonatic and mixed facies of the Sete Lagoas Formation and conglomeratic facies of the Carrancas

Tableau 1

Description synthétique des différents faciès identifiés dans la formation de Sete Lagoas (et du conglomérat de Carrancas)

| Lithology/facies	Structures	Process	Interpretation	Facies association
Matrix supported-polymitic conglomerate. Rounded to angular pebbles (Cm)	Massive, normal grading	Debris flow. Cementation of sparry calcite during diagenesis	Basement-incised channels	*FA1*
Pebbly sandstone with calcite cement (SMp)	Incipient evenly parallel lamination	Deposition by tractive currents inside incised channels		
Lime mudstone cementstone (Mc)	Crystal fans, fibrous crust laminae	Events of precipitation of aragonite crystals and crusts in the seafloor, concomitant with lime mud precipitation, associated with $CaCO_3$-supersaturated seawater in calm environment	$CaCO_3$-oversatureted deep platform	*FA2*
Lime mudstone (Mp)	Evenly parallel lamination	Precipitation of lime mud		
Crystalline limestone (Lh)	Swaley and hummocky cross-stratification. Interference ripples marks	Deposition by combined flow with predominance of oscillatory flow related to storm-wave action in the shoreface zone	Storm dominated middle ramp	*FA3*
Crystalline limestone (Lm)	Megaripple bedding with low-angle cross-stratification; mud drapes in the top of the bed forms; ripple marks; bed base scoured with centimetre-scale gutter cap	Subtidal bar migration under unidirectional tractive currents with intervals of slackwaters		
Crystalline limestone (Lc)	Supercritical wave climbing-ripples and quasi-planar lamination	Oscillatory and combined flow depositing from traction and suspension	Tide-dominated inner ramp	*FA4*
Crystalline limestone/pelite rhythmite (Rh)	Heterolithic bedding (wavy-flaser structures, mud drapes, mud couplets) asymmetric ripple marks	Migration of ripples with alternation of traction and suspension related to tidal currents in subtidal setting		
Crystalline limestone (Lp)	Plane-parallel lamination; gutter cast; asymmetric ripple marks; low-angle truncated lamination; channel geometry	Bar migration filling subtidal channels, possible influence of long-shore currents		
Lime mudstone/pelite rhythmite (Rmp)	Tabular layers	Alternation of carbonate precipitation and pelite deposition by suspension	Mixed carbonate siliciclastic outer ramp	*FA5*
Black crystalline limestone (Bp)	Planar lamination; wave truncated lamination; pinch and swell lamination	Deposition by wave action induced by storms in the shoreface zone; occasionally liquefaction	Wave-influenced stromatolitic inner ramp	*FA6*
Microbial boundstone (Mb)	Columnar, locally breached stromatolite with internal convex lamination	Microbial biologic activity associated to current action		
Black crystalline limestone (Bw)	Convolute and planar lamination	Rapid deposition on inclined surface followed by deformation by the movement of the unconsolidated sediment under the influence of gravity	Steepened carbonate outer ramp	*FA7*
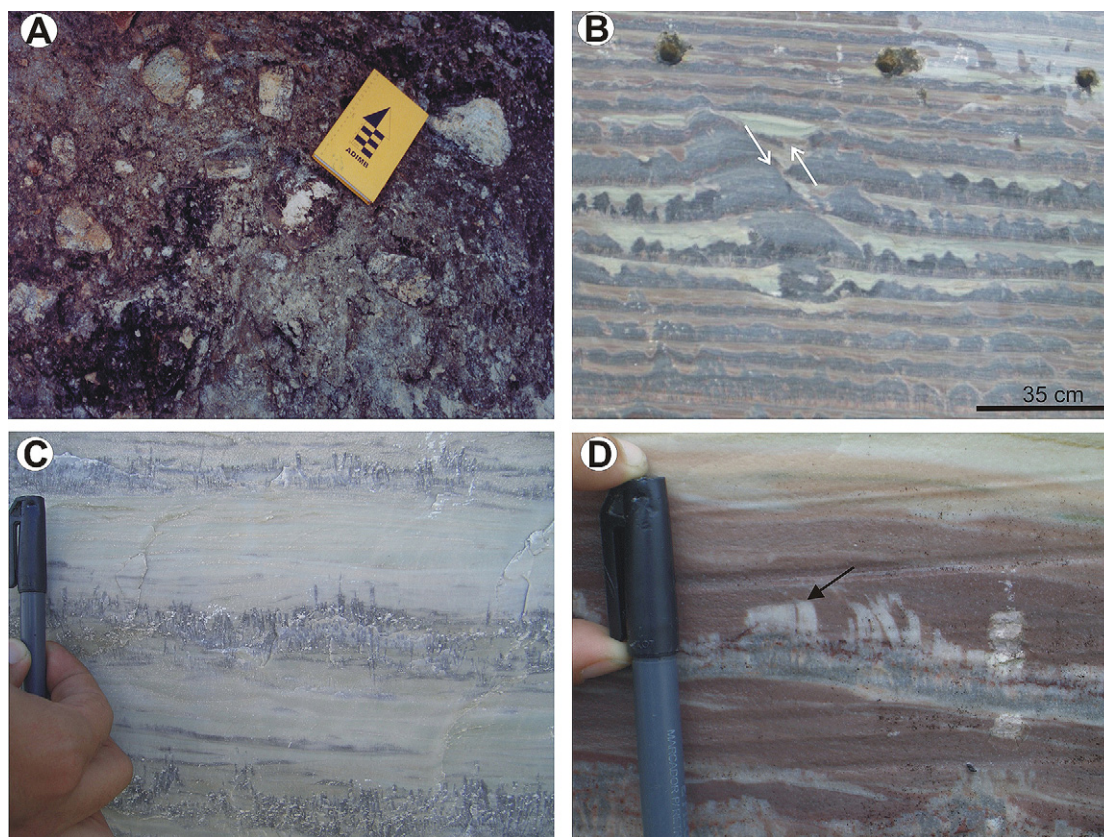
Fig. 2. Distinctive features of FA1 and FA2. (A) Matrix-supported polymictic conglomerate (diamictite) with rounded to angular pebbles of quartzite, gneiss and carbonate. In (C) and (D), the pen's cap is 4 cm long; in (A), the notebook is 18 cm long. (B) Centimetre-scale cycles of lime mudstone and calcite crystal fans (aragonite pseudomorph) displaced by synsedimentary faults (arrows). (C) Dark-grey aragonite-pseudomorph crystals with acicular morphology and straight terminations. Note (D) undulate laminations in micritic layers above white diagenetic crystal overgrowths (arrow) in crystal fans.

Fig. 2. Caractéristiques en mésoéchelle des associations de faciès FA1 et FA2.

crystalline limestone with quasi-planar to supercritical climbing wave-ripple cross lamination of the Lc facies.

The FA2 covers thousands of square kilometres in the study area, suggesting a wide platform setting, free from the action of strong currents in the initial stages of the Sete Lagoas succession. Preserved crystal fans are concentrated in beds, without any evidence of either wave or storm action corroborating a sub-wave storm environment. Aragonite crystal growth at the ocean floor has been ascribed to deep-platform environments associated with $CaCO_3$ oversaturation in the ocean [36,46,60]. Interestingly, periodic cycles of lime mudstone/cementstone precipitation could imply a recurrence in oversaturation events. The waning of crystal fans upsection, accompanied by the increase of wave structures, suggests a progressive change from a $CaCO_3$-oversaturated deep-water setting to the more energetic, moderately deep environment that characterizes the transition to FA3.

3.3. Storm-dominated middle ramp (FA3)

Storm-dominated middle ramp deposits comprise crystalline limestone with hummocky cross-stratification (Lh) and megaripple bedding (Lm).

Facies Lh and Lm are better exposed at the lower 20 m of the section PA and at the upper 40 m of section TA. They correspond to a set of undulating beds of grey and red crystalline limestone with mud drapes (Fig. 3A). Hummocky cross-stratification (wavelength up to 1.5 m) is observed, associated with pinch and swell lamination, quasi-planar lamination, and subordinately swaley cross-stratification. In plane view, hummocky domes are crowned by ripple marks with interference pattern (Fig. 3B). These deposits grade laterally to facies Lm exhibiting megaripple bedding with low-angle cross-stratification parted by mud drapes. The base of the beds is planar to erosive, with centimetre-scale gutter casts occurring frequently.
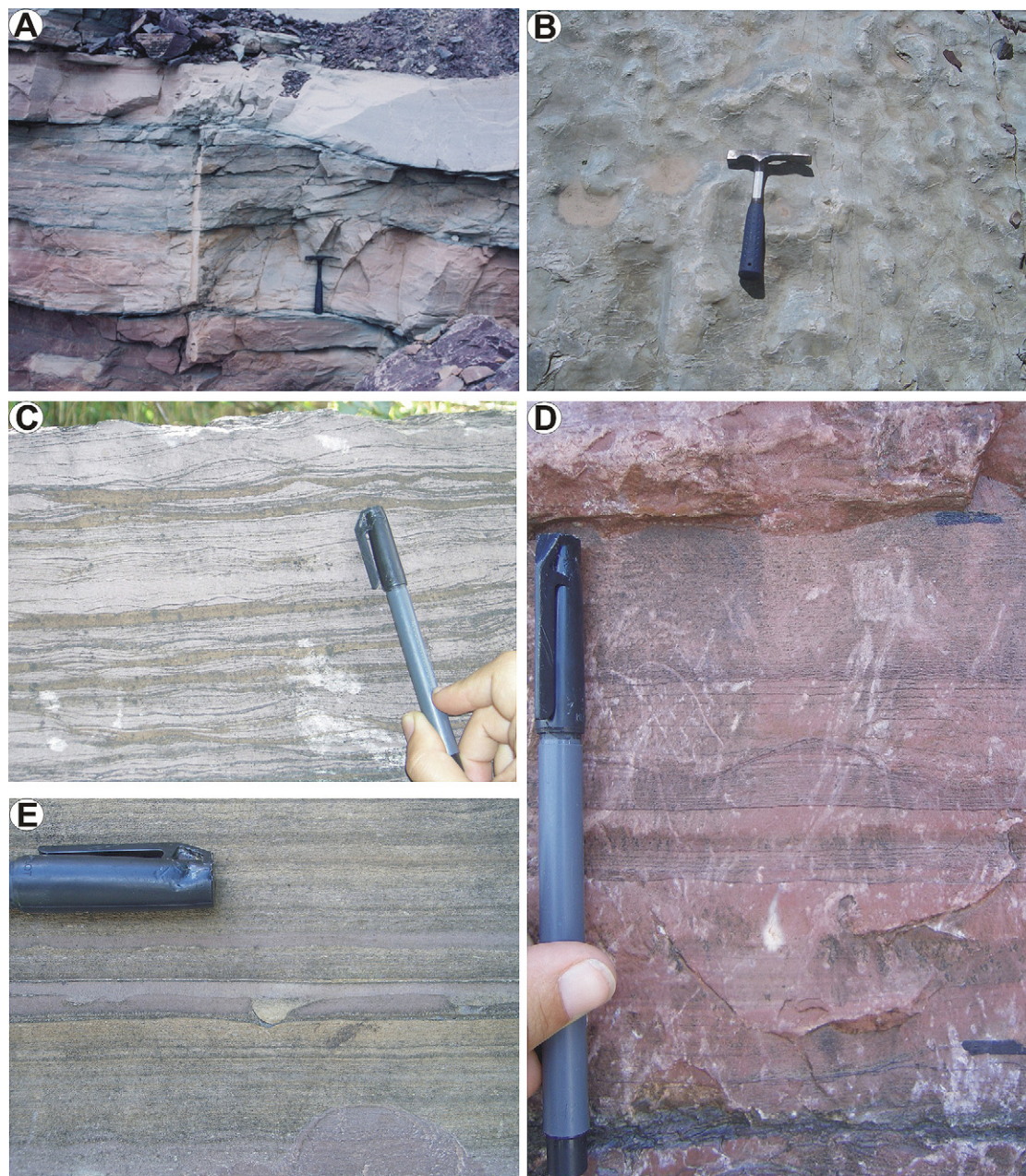
Fig. 3. Distinctive features of FA3 and FA4. (A) Undulating beds of grey and red crystalline limestone parted by mud drapes with low-angle truncation. (B) Ripple marks with interference pattern over hummocky domes. (C) Climbing-ripple cross lamination outlined by mud drapes. (D) Mud drapes separating thin and thick limestone laminae forming mud couplets, tidal rhythmite. (E) Evenly parallel lamination eroded by centimetre-scale gutter cast. In (A) and (B), the hammer is 35 cm long; in (C), (D) and (E), the pen's cap is 4 cm long.

Fig. 3. Caractéristiques en mésoéchelle des associations de faciès FA3 et FA4.

The coarse-grained nature of the deposits and the ubiquitous presence of terrigenous grains (up to 10%) associated with several types of lamination (planar, hummocky, and swaley) suggest a high-energy carbonate facies. The presence of hummocky cross-stratification and associated wave structures indicate storm-related, powered combined flow [9]. Mud partitions suggest deposition in lower shoreface. Large-scale bed forms with preserved morphology and scoured base (gutter cast) indicate periodic migration of megaripples or bars under current action with alternation of suspension, and sporadic storm events.

3.4. Tidal-dominated inner ramp (FA4)

Tidal-dominated inner ramp deposits comprise crystalline limestone with evenly parallel lamination (Lp), climbing ripples and quasi-planar lamination (Lc), forming rhythmite with pelite (Rh).

Facies Rh is characterized by heterolithic bedding of the reddish crystalline limestone and pelite rhythmite. This facies is observed exclusively at the PA section, distributed in tabular beds up to 40 cm thick, laterally extensive for more than hundreds of metres. Main structures are: wavy bedding, asymmetric ripple marks, and supercritical climbing-ripple cross lamination, generally outlined by mud drapes (Fig. 3C). The planar bedding is characterized by a strong regularity of mud drapes separating thin and thick limestone laminae, interpreted as mud couplets (Fig. 3D). Facies Rh alternates or is interbedded with an evenly parallel laminated-crystalline limestone (facies Lp), sometimes filling channels. Channels are tens of meters wide and less than five metres deep, asymmetric with planar-erosive, mud-draped base; some of them show a preserved flank. Inclined beds at the flank limb are conformable with the horizontal beds away from the channel. Locally, millimetre-scale gutter casts erode the planar lamination (Fig. 3E). Facies Lc is found above facies Rh and Lp. It consists of crystalline limestone with supercritical wave climbing ripples (up to 20 cm in thickness) and quasi-planar lamination. Aragonite-pseudomorph crystal fans are found associated with intertidal deposits.

Heterolithic beds indicate the alternation of traction and suspension controlled by tidal currents. The regular arrangement of rhythmite beds is interpreted as due to the alternation of slack waters and currents probably related to ebb/flood diary cycles, the thicker beds separated by mudstone layers being the highest tidal cycles. Migratory channels filled by shoals (even parallel laminated limestone) were incisive into the subtidal zone. The presence of aragonite-pseudomorph crystal fans at the top of the FA4 is interpreted as a shallow-water, saturation event in a restricted bay.

3.5. Mixed carbonate-siliciclastic outer ramp (FA5)

Mixed outer ramp deposits of FA5 comprise grey lime mudstone–pelite rhythmite (Rmp) and black crystalline limestone (Bp)s. They are the most expressive facies association in the study area, reaching up to 160 m in thickness at some sections, mostly in the southeastern sector of the study area. The Rmp is formed by the alternation of carbonate and pelite, and reaches more than 12 m in thickness (Fig. 4A and B). Individual beds vary from 2 to 15 cm in thickness. This facies grades upward to the thick succession of black limestones of facies Bp (Fig. 4A), which is characterized by planar to low-angle lamination and high organic matter content.

The large surface covered by FA5 throughout the study area indicates a wide platform setting. The abundance of fine siliclastic at the basal unit suggests a deepest-offshore zone where carbonate precipitation is limited. Moreover, the lack of wave structures and the upward presence of laminated crystalline limestone (originally mudstone), rich in organic matter, corroborates the continuous deposition in deep waters.

3.6. Wave-influenced inner ramp (FA6)

Deposits of FA6 comprise two facies: black crystalline limestone with planar and wave truncated lamination (Bp), and microbial boundstone (Mb). Facies Bp is characterized by wave-truncated lamination (wavelength up to 60 cm and 5 cm high) with undulated internal lamination forming pinch and swell arrays. Individual beds are 15 cm thick, and exhibit in the base a small-scale gutter cast. Convolute bedding occurs locally. Facies Mb was observed only in section PR, and corresponds to dark grey to black columnar, rarely branching stromatolites (Fig. 4C). Individual columns are up to 40 cm and can be as large as 10 cm in diameter, with convex internal lamination. In transverse section, they display a polygonal morphology, the inter-column spaces being filled by black lime mudstone or locally brecciated.

Ubiquitous truncated laminations and planar laminations suggest wave action in upper regime flow (e.g., [28]), probably induced by storms in the shoreface zone. Liquefaction processes are attributed to the wave impact in unconsolidated sediments. Microbial mat colonization occurred in low-energy zones with deposition of carbonate muds related to shallow subtidal or lagoon environment. Locally, the collapse of stromatolites generated intraformational breccias filling inter-column depressions.

3.7. Steepened carbonate outer ramp (FA7)

Deposits of FA7 represent a deeper, lateral variation of FA6. They comprise black crystalline limestone with convolute and planar lamination (Bw). Deformational features include also slump folds and slight undulation of planar lamination. Convoluted layers are 2 to 10 cm thick. These layers are interbedded with non-deformed layers, forming deposits of tens of metres in thickness. The abundance of deformational features (convolute
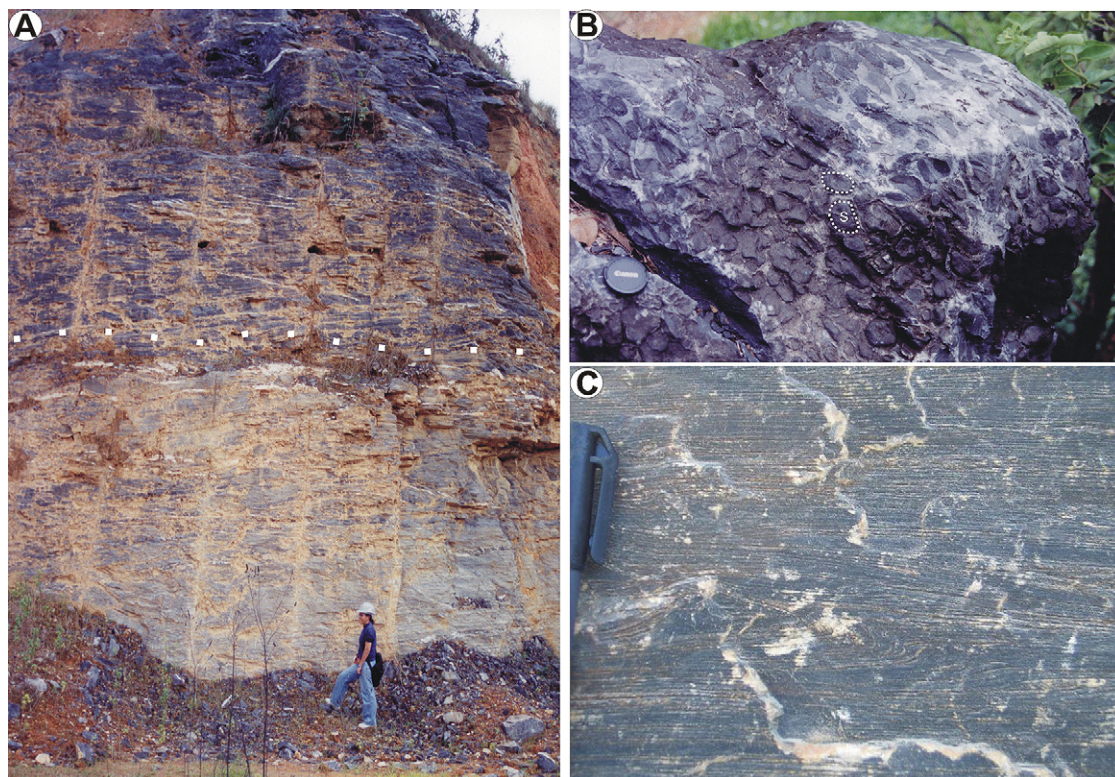
Fig. 4. Distinctive features of FA5 and FA6. (A) Contact, dashed line, between the lime mudstone–pelite rhythmite and black crystalline limestone in the CA section. (B) Lime mudstone–pelite rhythmite in the MG section. Pelite beds vanish towards the top, where lime mudstone–pelite rhythmite grades to crystalline black limestone of facies Bp. (C) Collumnar stromatolites (S) in plane view; dotted lines delineate two columns. In (A), the character is 1,55 m tall; in (B), the lens cap is 6 cm in diameter. In (C), the pen's cap is 4 cm long.

Fig. 4. Caractéristiques en mésoéchelle des associations de faciès FA5 et FA6.

lamination, slump folds) suggests a rapid deposition in a steepened ramp setting.

It is worth noting that black limestones are found into facies associations FA5, FA6, and FA7 (comprising facies Bp, Bw and Mb), and may reach altogether up to 200 m in thickness. Obliteration of primary structures by recrystallization may hinder individualization of such a facies in the field.

4. Isotopes

C and O isotope analyses were performed in 232 (Table 2) fine-grained limestone samples from sections LO, SA, PA, TA, CA, PR, MG, CE, and CR (Fig. 5). For our analysis, homogeneous rock fractions were preferred, whereas fractured, mineral-filled and weathered zones were avoided. The analyzed samples are fresh and show no trace of deformation or intensive neomorphism. In thin section, the original texture is usually preserved, even though neomorphic modifications locally occur, such as the calcite tuffs considered to

be aragonite pseudomorphs found in facies Mc (FA2, Fig. 2) and the recrystallization observed in facies Rmp, Bp and Mb (FA6, FA7; Fig. 4).

Analyses were carried out at the Stable Isotopes Lab of the Geochronological Research Centre, University of São Paulo, Brazil (CPGEO/USP). CO_2 gas was extracted from powdered carbonates in a high-vacuum line after reaction with 100% phosphoric acid at room temperature for 24 h. Following cryogenic cleaning, the released CO_2 was analyzed in a EUROPA, GEO 20–20 mass spectrometer, using IAEA standards as well as secondary standards. Results for both carbon and oxygen are reported in conventional notation in per mil (‰) relative to the PDB (Pee Dee Belemnites) standard. The uncertainties of isotope measurements are 0.2‰ for both carbon and oxygen.

4.1. Carbon isotopes

The carbon isotope record shows coherent and phased changes corresponding to the stratigraphic

Table 2
δ^{13}C and δ^{18}O values of the Sete Lagoas Formation and conglomeratic (matrix) facies of the Carrancas unit

Tableau 2
Valeurs de δ^{13}C et δ^{18}O pour la formation de Sete Lagoas et le conglomérat de Carrancas

Section	Sample	δ^{13}C ‰ (PDB)	δ^{18}O ‰ (PDB)	Sample	δ^{13}C ‰ (PDB)	δ^{18}O ‰ (PDB)
Carrancas (CR)	I.1.–1	−4.08	−12.03	I.1.1.15	−3.17	−11.75
	I.1.–1.4	−5.04	−13.55	I.1.1.25	−3.42	−11.91
	I.1.–1.6	−4.67	−12.03	I.1.1.34	−3.00	−11.48
	I.1.–1.20	−4.59	−12.27	I.1.1.35	−2.30	−10.99
	I.1.0	−3.36	−12.22	I.1.1.55	−3.11	−8.910
	I.1.0.55	−3.01	−13.10	I.1.1.75	−2.13	−11.83
	I.1.0.75	−3.49	−11.37	I.1.1.95	−3.12	−11.17
	I.1.0.95	−2.76	−13.41			
Canaã (CA)	I.2.1	4.58	−8.36	I.2.22	8.32	−6.66
	I.2.10	3.14	−8.83	I.2.23	8.73	−6.67
	I.2.11	3.35	−8.64	I.2.24	8.36	−7.06
	I.2.12	3.38	−8.71	I.2.25	8.59	−6.72
	I.2.13	3.98	−7.69	I.2.26	8.54	−6.67
	I.2.15	4.46	−8.39	I.2.27	8.12	−8.36
	I.2.16	4.12	−9.02	I.2.28	9.517	−6.61
	I.2.19	7.99	−8.16	I.2.29	9.537	−9.54
	I.2.20	8.14	−9.27	I.2.30	9.35	−7.55
Sambra (SA)	TMG13	−4.48	−9.92	TMG24	0.08	−6.79
	TMG14	−4.10	−9.48	TMG25	−0.066	−7.083
	TMG15	−4.15	−8.73	TMG26	−0.11	−6.11
	TMG16	−3.82	−7.76	TMG27	−0.206	−5.99
	TMG17	−3.749	−8.224	TMG28	−0.21	−5.99
	TMG18	−3.12	−7.32	TMG29	0.54	−5.67
	TMG19	−2.193	−7.88	TMG30	0.37	−6.65
	TMG20	−0.72	−8.23	TMG31	1.00	−5.27
	TMG21	−0.38	−7.59	TMG32	0.28	−7.85
	TMG22	0.80	−8.01	TMG33	−0.26	−7.28
	TMG23	0.29	−7.95			
Policia Rodoviária (PR)	I.5.1	10.89	−9.59	I.5.5	11.20	−9.92
	I.5.2	11.81	−7.79	I.5.6	11.42	−10.70
	I.5.3	10.62	−10.42	I.5.7	10.45	−12.03
	I.5.4	10.93	−10.66	I.5.8	10.50	−12.47
Paraiso (PA)	LU.7.0'	−0.15	−6.71	LU.7.7.50	0.54	−7.01
	LU.7.0	0.23	−7.69	LU.7.8'	0.37	−5.71
	LU.7.1'	−0.57	−7.45	LU.7.9.5	0.68	−7.05
	LU.7.1.20	0.44	−7.18	LU.7.10'	−0.48	−6.98
	LU.7.2.20	0.45	−7.15	LU.7.10.5	1.05	−6.58
	LU.7.3'	0.60	−5.87	LU.7.12'	−0.67	−7.19
	LU.7.4'	0.70	−5.88	LU.7.14'	−0.65	−7.20
	LU.7.5.20	0.516	−7.03	LU.7.15'	−0.86	−7.38
	LU.7.6.20	0.36	−7.24	LU.7.16'	−0.47	−6.94
	LU.7.6'	−0.42	−6.99	LU.7.19'	−0.85	−7.49
Mata Grande (MG)	I.8.1	2.41	−9.86	I.8.17	8.22	−6.44
	I.8.2	3.66	−10.04	I.8.18	8.39	−6.49
	I.8.3	3.81	−10.24	I.8.19	8.62	−7.04
	I.8.5	4.05	−7.13	I.8.20	8.01	−6.99
	I.8.6	5.51	−8.19	I.8.21	8.64	−7.03
	I.8.8	1.10	−8.25	I.8.25	8.69	−7.40
	I.8.10	5.75	−8.34	I.8.31	9.19	−6.11
	I.8.11	6.78	−7.53	I.8.32	9.20	−8.24
	I.8.13	8.12	−6.22	I.8.35	7.59	−8.04
	I.8.14	8.36	−5.75	I.8.37	8.77	−7.91
	I.8.16	8.60	−5.73	I.8.39	9.21	−7.54

Table 2 (*Continued*)
Tableau 2 (Suite)

| Section	Sample	$\delta^{13}C$ ‰ (PDB)	$\delta^{18}O$ ‰ (PDB)	Sample	$\delta^{13}C$ ‰ (PDB)	$\delta^{18}O$ ‰ (PDB)
	I.8.62	9.425	−7.802	I.8.107	10.01	−9.97
	I.8.65	8.46	−7.88	I.8.111	10.19	−10.39
	I.8.68	9.40	−8.02	I.8.112	10.29	−10.75
	I.8.70	10.246	−7.92	I.8.113	10.79	−10.65
	I.8.75	9.86	−8.41	I.8.114	11.89	−12.05
	I.8.78	9.56	−9.03	I.8.117	10.83	−11.41
	I.8.81	9.38	−10.12	I.8.119	11.87	−10.67
	I.8.85	9.95	−9.99	I.8.120	10.78	−11.07
	I.8.88	9.83	−10.82	I.8.121	13.36	−11.49
	I.8.90	10.43	−9.62	I.8.122	12.51	−12.55
	I.8.91	10.05	−10.27	I.8.123	11.31	−9.39
Mata Grande (MG)	I.8.92	10.19	−10.76	I.8.125	11.67	−11.15
	I.8.93	9.67	−10.76	I.8.126	9.85	−12.34
	I.8.94	9.43	−10.30	I.8.134	10.82	−9.69
	I.8.95	10.13	−9.52	I.8.135	10.64	−11.10
	I.8.96	9.89	−10.89	I.8.137	14.65	−10.29
	I.8.101	10.36	−10.49	I.8.140	10.01	−10.62
	I.8.102	6.93	−6.92	I.8.144	12.32	−11.74
	I.8.103	10.25	−10.56	I.8.145	11.73	−12.58
	I.8.104	9.91	−11.24	I.8.153	11.79	−11.14
	I.8.105	10.80	−9.56	I.8.154	11.09	−12.57
	I.8.62	9.425	−7.802			
	I.9.1	−0.70	−7.73	I.9.16	−0.16	−7.37
	I.9.2	−0.18	−7.34	I.9.17	1.50	−6.62
	I.9.4	−0.03	−7.20	I.9.18	0.15	−7.15
	I.9.5	−0.47	−7.47	I.9.19	−0.01	−7.35
	I.9.6	−0.29	−7.40	I.9.20	−0.46	−7.50
	I.9.7	0.11	−7.28	I.9.21	−0.46	−7.52
	I.9.8	0.43	−7.16	I.9.22	−0.44	−7.67
	I.9.9	−0.15	−7.45	I.9.23	−0.02	−7.40
	I.9.10	−0.67	−7.52	I.9.24	−0.23	−7.59
Lontra (LO)	I.9.11	−0.23	−7.51	LU.9.2.6	9.65	−5.79
	I.9.12	1.22	−6.70	LU.9.2.7	3.13	−7.54
	I.9.13	1.46	−6.53	LU.9.2.8	3.18	−7.42
	I.9.14	0.09	−7.21	LU.9.2.9	1.41	−7.50
	I.9.15	−0.20	−7.29	LU.9.2.10	1.30	−7.46
	LU.10.4'	−2.82	−10.65	LU.10.16'	−0.05	−7.33
	LU.10.5'	−1.75	−10.32	LU.10.18'	−0.45	−7.33
	LU.10.6'	0.60	−8.64	LU.10.19'	−0.28	−7.31
	LU.10.7'	0.78	−8.22	LU.10.20'	−0.32	−7.12
	LU.10.8'	0.77	−8.14	LU.10.21'	−0.26	−7.57
Tatiana (TA)	LU.10.9'	−0.12	−8.03	LU.10.22'	0.41	−6.80
	LU.10.10'	0.29	−7.70	LU.10.25	−0.47	−6.97
	LU.10.11'	0.13	−7.81	LU.10.30	−0.26	−7.05
	LU.10.12'	−0.12	−7.80	LU.10.35	−0.40	−6.99
	LU.10.13'	−0.09	−7.79	LU.10.40	−0.14	−7.22
	LU.10.14'	0.09	−7.70	LU.10.45	0.64	−8.03
	LU.10.15'	−0.308	−7.507			
	I.12.(−2.80)	−2.57	−12.12	I.12.16	0.23	−8.48
	I.12.(−1.77)	−2.58	−11.53	I.12.18	0.17	−8.24
	I.12.(−1.40)	−1.95	−10.82	I.12.22	0.81	−7.83
	I.12.(−0.40)	−0.50	−10.30			
	I.12.0	−1.24	−11.46	I.12.24	0.82	−7.95
	I.12.1	−0.22	−10.05	I.12.26	0.82	−8.00
	I.12.2	−0.92	−10.40	I.12.36	1.22	−7.30
	I.12.3	−0.79	−10.11	I.12.38	1.16	−7.43
Cauê (CE)	I.12.4	−1.12	−10.05	I.12.40	1.19	−7.37
	I.12.5	−0.87	−10.44	I.12.42	1.32	−7.28

Table 2 (*Continued*)
Tableau 2 (Suite)

Section	Sample	δ^{13}C ‰ (PDB)	δ^{18}O ‰ (PDB)	Sample	δ^{13}C ‰ (PDB)	δ^{18}O ‰ (PDB)
	I.12.6	−0.84	−10.36	I.12.52	8.40	−5.36
	I.12.7	−0.82	−9.86	I.12.54	7.60	−8.36
	I.12.8	−0.83	−9.82	I.12.56	7.92	−6.65
	I.12.9	−0.93	−9.68	I.12.58	8.30	−5.70
	I.12.10	−0.85	−9.29	I.12.60	8.31	−4.79
	I.12.12	−0.46	−8.39	I.12.62	8.33	−5.54
	I.12.14	0.04	−8.52	I.12.64	8.44	−5.23

variations (Fig. 5). The δ^{13}C-δ^{18}O cross-plot in Fig. 6 clearly shows a net increase in δ^{13}C towards the top of the succession (from FA1 to FA7), with distinct clusters of samples for contemporary facies association. The carbonate matrix of the Carrancas conglomerate (FA1) shows the most depleted δ^{13}C, ranging from –5.1 to –3.3‰. The lowermost sectors of sections CR, SA and TA (FA2), comprising lime mudstones with aragonite pseudormorphs, show depleted δ^{13}C values around –4‰. Upsection, these values increase from –4.5

to + 0.8‰. In sections TA and CE, δ^{13}C values increase sharply to around 0‰ within the first metre of the facies association FA2, and remain constant within facies association FA3. In section SA, δ^{13}C values increase gradually (within 20 m), reaching the value of 0‰ at the base of the facies association FA3 (Fig. 5). The presence of rocks from FA2 with values around 0‰ is responsible for the overlapping of isotopic values between FA2 and FA3 (oversaturated outer ramp and storm-dominated middle ramp) in Fig. 6. Values of δ^{13}C for FA3 and FA4
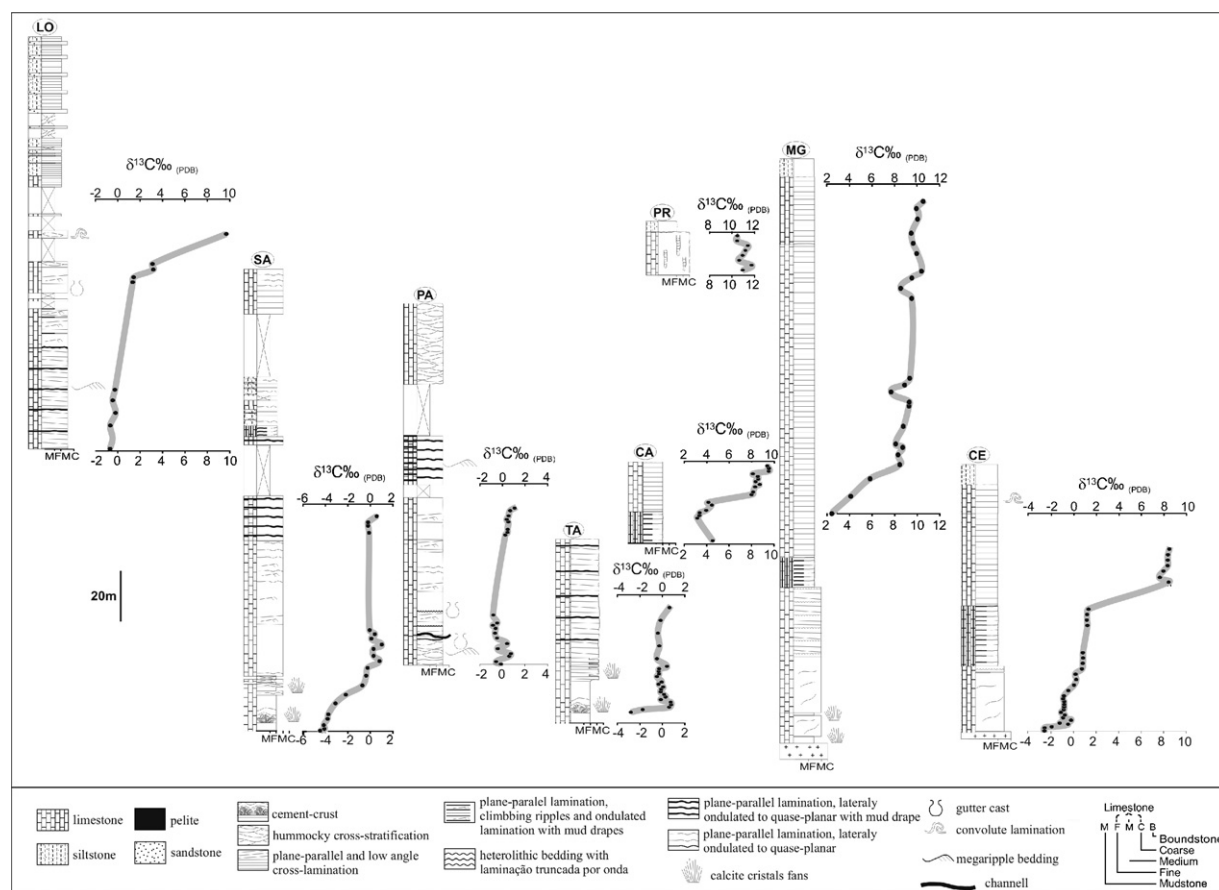
Fig. 5. Stratigraphic sections of the Sete Lagoas Formation coupled with δ^{13}C profiles. Isotopic values are in ‰.

Fig. 5. Sections stratigraphiques de la formation Sete Lagoas, avec profils du δ^{13}C. Les valeurs isotopiques sont données en ‰.
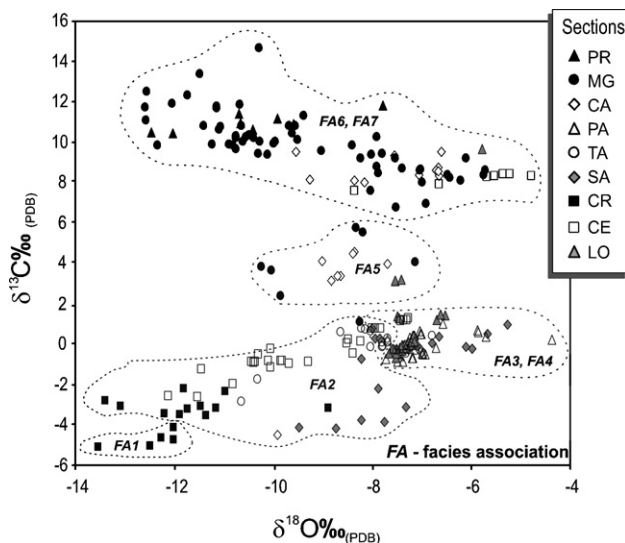
Fig. 6. δ^{13}C versus δ^{18}O cross-plots for facies associations (FA1, FA2, FA3, and FA4, FA5, FA6,FA7) of the Sete Lagoas carbonate succession and Carrancas conglomerate. Isotopic values are in ‰.

Fig. 6. Diagramme (δ^{13}C–δ^{18}O) pour les différentes associations de faciès (FA1, FA2, FA3 et FA4, FA5, FA6, FA7) de la succession carbonatée de Sete Lagoas et du conglomérat Carrancas. Les valeurs isotopiques sont données en ‰.

are limited to a narrow range around 0‰ (Fig. 5). Facies association FA5 is characterized by positive δ^{13}C values. These values increase from around +2‰ in the lowermost mudstone–pelite rhythmite to values in excess of +8‰ in the uppermost black mudstone of FA6 and FA7 (Fig. 5). The microbial boundstone of FA6, which caps the carbonate succession of the Sete Lagoas Formation, shows high δ^{13}C values varying from +10.5 up to +11.2‰, and the highest δ^{13}C value of +14.3‰ is found in the black limestone of FA5.

4.2. Oxygen isotopes

The oxygen record shows a large spread with δ^{18}O varying from –14 up to –6‰. But, in contrast to the carbon isotopes, it shows large variations and little overlap among the sections (Fig. 6). For instance, facies association FA2 was sampled in three sections (CR, SA, and TA) and shows a large variation in δ^{18}O values (ranging from –13.1 to –7.3‰), but values for each sampled outcrop seem to cluster within 2‰: in the CR section, δ^{18}O values vary between –13.1 and –11.2‰, whereas values for section TA are between –10.6 and 7.5‰, and values for section SA are between –9.9 and –7.3‰. Similarly, facies associations FA6 and FA7 show a wide range of δ^{18}O values, from –12.0 to –5.7‰, with narrower and specific ranges for PR, CA, and MG sections. Nonetheless, some sections show a coherent trend in δ^{18}O values, with less negative values towards the top. This is the case of section SA, for which values

of –9.9‰ were obtained on limestones with aragonite-pseudomorph crystal fans at the base of the outcrop, contrasting with the values of –5.7‰ obtained on the storm-dominated crystalline limestone at the top.

In summary, in the Sete Lagoas Formation, the oxygen isotope ratios (δ^{18}O) for most sections seem to record local signatures. This and the much depleted values, between –13.5 to –4.5‰, suggest some degree of diagenetic imprint on the oxygen isotopic signal, despite the apparent pristine state of the samples. Therefore, the O isotope values will not be used in the discussion.

5. Discussion

5.1. Depositional model and evolution of the Sete Lagoas carbonate platform

The stratigraphic and sedimentologic data presented above allowed us to develop a depositional model for the Sete Lagoas carbonate platform and thus to establish a framework for regional correlation. The carbonate platform developed on the Palaeoproterozoic basement, preserving the Carrancas conglomerate in isolated channels. The Carrancas conglomerate (FA1) defines a metre-scale thinning-upward cycle, possibly of coastal to alluvial origin, with no evidence of a glaciogenic environment. It is interpreted as representing the initial stages of platform development. Then, the palaeoenvironmental interpretation reveals a deep- to shallow-

platform setting, with a depocentre towards the south-eastern border of the São Francisco craton, as indicated by the thickness increase of deep-water deposits (and the thinning of shallow-water deposits) to the southeast (Fig. 5). Preservation of a thick shallow-water succession in some sections suggests a strongly subsiding basin, and the presence of storm- and tide-influenced deposits indicates an oceanic connection.

Two shallowing-upward megacycles are recognized, comprising more than 200 m in the stratigraphic record. Each cycle is limited by a flooding surface amalgamated with a third-order sequence boundary [52].
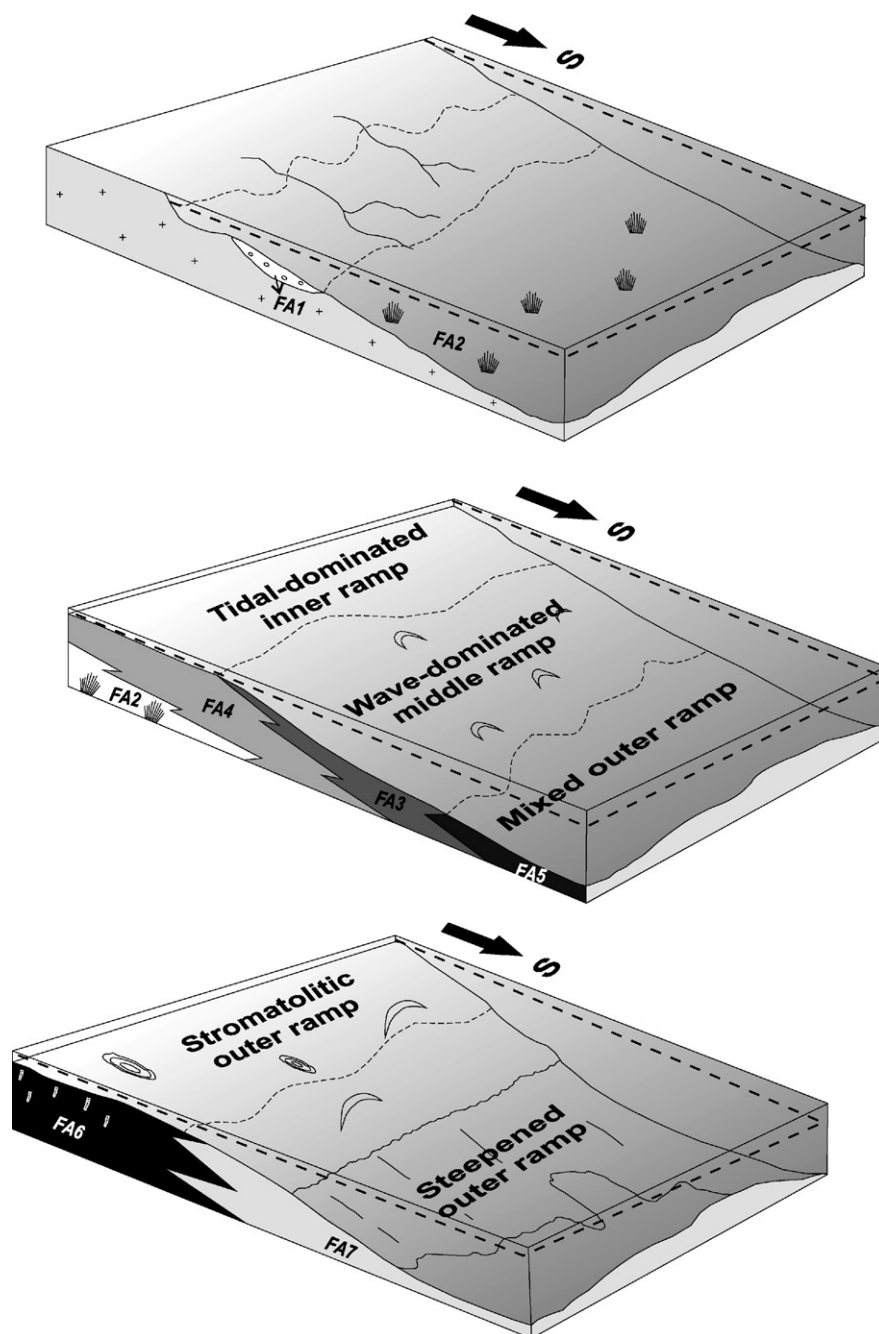

Fig. 7. 3-D Sketches showing facies relationships in different sections of the Sete Lagoas carbonate platform.

Fig. 7. Blocs-diagrammes montrant l'évolution de la sédimentation dans la plate-forme de Sete Lagoas.

The first megacycle (Fig. 7a) begins with deep-water deposition in an aragonitic, oversaturated ocean (FA2). It marks a pronounced transgression over the São Francisco craton, depositing carbonates over the Carrancas conglomerate or the basement rocks. The oversaturated waters enabled the periodic nucleation of seafloor precipitates, including crystal fans and crusts, covered by micrite. Furthermore, during the highstand, tide- and storm-influenced deposition (FA3 and FA4) prevailed. At this stage, deposition along the coast of the Sete Lagoas platform seems to have been strongly controlled by storm waves, but tidal processes dominated in locally protected zones (Fig. 7b).

The second megacycle (Fig. 7c) starts with a transgression, drowning the platform and allowing deposition of a thick succession of mixed, sub-storm wave-base deposits (FA5). It contrasts sharply with the first one by the lack of oversaturation events and the larger volume of deposits. We note also the lack of cyclicity and exposure surfaces throughout more than 200 m in the sedimentary record, suggesting high subsidence rates of the basin at this stage. This deep-water environment was prone to organic-matter preservation in the black limestones (upper FA5, FA6, and FA7). Coastal environments were developed after the progressive shallowing of the basin, forming fair-weather wave and storm deposits, associated with microbial building (FA6). Towards the depocentre, these rocks present ubiquitous deformational features, such as convolute and undulated laminations (FA7), related to the steepening of the ramp morphology. This megacycle ends with a rapid transgression marked by the deposition of siltstones and sandstones of the Santa Helena Formation.

5.2. Evolution of C isotopic composition in the Sete Lagoas platform

In the Neoproterozoic successions, correlations rely mostly on the carbonate $\delta^{13}C$ variations, on the basis of the hypothesis that the $\delta^{13}C$ of carbonates is primary and records the $\delta^{13}C$ of dissolved inorganic carbon in the surface oceans, considered to be homogeneous at the geological scale. Although the $\delta^{13}C$ composition in carbonate rocks is quite resistant to chemical over-printing, as many studies have indicated that even diagenetically altered carbonates appear to preserve their original $\delta^{13}C$ [7,20,27,39,40], care must be taken to ensure that it is the case.

As already mentioned, the Sete Lagoas Formation has not undergone metamorphism and the selected samples show little evidence for carbonate mineral neomorphism, except in the Carrancas conglomerate (FA1), which will not be considered in the following discussion. Here, the absence of covariations of $\delta^{13}C$ with $\delta^{18}O$ within and between each facies association, and the fact that $\delta^{13}C$ presents very similar values for each facies association, independently of the section (Fig. 6), strongly suggest that $\delta^{13}C$ records a primary signature. Moreover, the carbon isotope difference between the carbonate and TOC of the Sete Lagoas Formation is constant and of 28 ± 2‰ [34], reinforcing the hypothesis of primary carbon signature preservation. The carbon isotope data reported here can therefore be interpreted as representing the original depositional signature and can be used for correlations with other Neoproterozoic sections worldwide.

The high-resolution $\delta^{13}C$ stratigraphy reported in this study shows a strong increase from the base to the top (between –4.5 and +14‰) of the Sete Lagoas Formation, consistent with previous data [34]. Such an isotopic variation is in agreement with the $\delta^{13}C$ signature found in the post-Sturtian sequences, where negative values in the cap carbonates directly overlying the diamictites are followed by extreme positive values upsection – see review in [27]. In fact, to our knowledge, such high $\delta^{13}C$ values have never been found in post-Marinoan sequences, which usually reach maximum values of +7 up to +10‰ [27,29,48,59].

The $\delta^{13}C$ stratigraphic record of the Sete Lagoas platform compares very well with other post-Sturtian successions, suggesting that the negative and positive excursions identified elsewhere are also recorded in the São Francisco Craton [61], and supporting the hypothesis that they are of global extent.

Considering a steady-state carbon cycle [29,45,58], some mechanisms have been invoked to explain the anomalous positive and negative shifts found in the $\delta^{13}C$ Neoproterozoic signature.

The global extension of the negative excursion that follows the Sturtian deglaciation seems to be quite established and usually occurs within cap carbonates. The mechanisms responsible for it are still a matter of debate – see review in [32].

The possible factors responsible for the positive excursion have been reviewed by Shields et al. [58]. The first hypothesis is anomalously high burial rates of isotopically depleted carbon as organic matter (enriching the shallow ocean in ^{13}C), but it has not been supported so far by known outcrops of organic-rich formations at this period. The second hypothesis is an increase in the isotopic composition of carbon entering the ocean due to the repetition of glacially related eustatic regressions. The third hypothesis is an increase

in the average isotopic fractionation between sedimentary carbonates and total organic carbon ($\Delta^{13}C_{carb\ org}$ comprised between 33 and 37‰), but it is insufficient on its own to explain the positive $\delta^{13}C$ excursions. The fourth hypothesis is that the high $\delta^{13}C$ is the result of unrepresentative sampling in restricted basins with locally elevated $\delta^{13}C$.

The Sete Lagoas formation is located in a different continent/sedimentary basin than those previously studied are [61], and it provides an additional record of the positive excursion, suggesting that this excursion is of global significance. In the Sete Lagoas Formation, $\delta^{13}C$ reaches unusually high values (up to + 14‰), which suggests an additional local control. For the first time, this unit provides geological evidence for high organic carbon burial rates, associated with high $\delta^{13}C$ values (up to 5% TOC [34]). Due to this high TOC, anoxia can be suspected and, indeed, some authors [34,58] have pointed out that the positive C isotope excursion seems to coincide with ocean redox stratification, with a causal mechanism remaining to decipher.

5.3. Recognition of a Sturtian carbonate

The presence of aragonite-pseudomorph crystal fans and other sedimentary features, associated with negative C-isotope excursions in Neoproterozoic transgressive carbonate successions following glacial deposition, has been used as a diagnostic of cap-carbonate deposits worldwide [33,40], despite some criticisms [46].

Cap-carbonate sequences found in different countries (Australia, Africa, China, Canada, India) display successions that present similar structures, depositional environments and isotopic signature (e.g. [27,32]). These successions typically show a transgressive cycle, which starts with cap dolostones constituted by fine, deep-water deposits [3,36,37,41]. They grade upward to disturbed platform facies [37,38] or grainstones and stromatolites near to the coast [13,36,41]. The $\delta^{13}C$ curves obtained on the cap carbonates show depleted $\delta^{13}C$ values (down to –6‰) at the bottom of the sequence, which increase upward to positive values [15,17,23,27,32,35,37,63].

Although cap-carbonate features have been described in a generical way [41] for sequences correlated to all Neoproterozoic glacial events (Sturtian, Marinoan, and Gaskiers), several differences have been observed between the cap carbonates following each glacial interval [42]. Most cap carbonates described in detail in the literature are correlated to post-Marinoan

deposition [3,26,36,64]. There are quite few detailed descriptions of cap carbonates related to the Sturtian event. Most post-Sturtian sequences are truncated at the bottom and lack a cap dolostone unit [24,32,42]. Post-Sturtian cap carbonates studied in northern Canada, southern Australia, and northern Namibia present successions initiated with a record of maximum flooding, which comprise either marly shales or rhythmites of black limestones rich in organic-matter or sulphide. They grade into allodapic dolomites, thin sandstone layers and slump breccias (southern Australia and Canada), and may also comprise stromatolites (Namibia). The carbon isotopic signature of post-Sturtian cap carbonates is also different from the post-Marinoan one due to their basal truncation [15,27,30]. Normally, the older (Sturtian) cap carbonates initiate with $\delta^{13}C$ values around –3‰ to –4‰, which rise quickly upward to positive values.

There is no firm evidence for glacial deposition below the carbonate deposits in the study area, the Carrancas conglomerate being interpreted here as a coastal-to-alluvial deposit infilling incised valleys. However, glaciogenic or glacially influenced units were recognized below the Bambuí Group in other regions of the São Francisco Craton, including the Jequitaí Formation [50,62] and the lower successions of the Macaúbas Group [38,62]. These units are probably a lateral equivalent to the basal unconformity of the Bambuí Group in the studied area. The FA2 may therefore represent a true cap carbonate, due to this regional correlation. In addition, the Sete Lagoas cap carbonate constitutes a transgressive sequence, beginning with the FA2 deep platform deposits characterized by $\delta^{13}C$ values of –4.5‰. These deposits grade upward to shallow platform deposits influenced by storm and wave, with $\delta^{13}C$ values around 0‰ (FA3 and FA4). All these features allow us to propose that the Sete Lagoas formation is a cap-carbonate sequence.

Because the rocks of the Sete Lagoas Formation were deformed during the Brasiliano event (630 Ma: [12]), which is older or contemporary with the recently obtained ages of the Marinoan glaciations (630 Ma: [11,31,64]), a Sturtian correlation seems better for the Sete Lagaos cap carbonate, and is also consistent with the $\delta^{13}C$ stratigraphy and the Pb–Pb age cited above (section 2).

However, comparison of the Sete Lagoas sedimentary and isotopic records with other Sturtian units raises some problems. The sedimentary record of Sete Lagoas resembles more that of post-Marinoan deposits. The base of the studied succession is marked by a thick interval (up to 16 m) with aragonite-pseudomorph

crystal fans that do not occur frequently in post-Sturtian cap carbonates. Aragonite-pseudomorph crystal fans in purported post-Sturtian deposits are described only in the Pocatello Formation, for which no basal glacial layer has been identified [22]. Moreover, in Sete Lagoas, the whole transgressive cycle is recorded; the maximum-flooding surface occupies the middle of the succession, where C-isotopic values shift from negative to positive. In other post-Sturtian carbonates, the record initiates with the maximum-flooding deposits and the transition of negative to positive C-isotopic values is located above the maximum-flooding surface.

Recent geochronological data available for ash beds within Neoproterozoic deposits point to a possible diachronism of glacial units usually correlated to the Sturtian event (709 ± 5 Ma, southeastern Idaho; 711.8 ± 1.6 Ma, Oman; 685 ± 7 Ma and 684 ± 4 Ma, central Idaho; 761 ± 8 Ma, southern China: see [22]). In this case, the Sete Lagoas carbonate platform does not necessarily correlate with other carbonate sequences in a worldwide basis, and the negative C anomaly could be of local significance. On the other hand, if we take the post-Sturtian sequences as coeval, differences in depositional settings may indicate different position/depths of sediment accumulation across the basin. Then, the Sete Lagoas succession would correspond to a shallower deposition with regard to other described post-Sturtian cap carbonates, and, because of that, it would present the record of wave-storm influenced deposition, which is not normally found in other post-Sturtian successions. In such case, the negative anomaly found at the base of Sete Lagoas succession would correlate with that found in southern Australia, Canada and Namibia.

6. Conclusion

The Sete Lagoas succession has been described at the southern tip of the São Francisco craton (its classical outcropping region), on the basis of facies analysis, stratigraphy and C-isotope signatures. It was subdivided into seven facies associations in a carbonate platform setting, forming two shallowing-upward megacycles. The first megacycle formed in a $CaCO_3$-oversaturated deep-platform, and ends up with storm- and tide-influenced deposits. The second megacycle is formed by thick, mixed deep- and shallow-platform deposits rich in organic matter. The two megacycles show characteristic C isotope signatures. The first transgressive deposits, rich in aragonite seafloor precipitates, exhibit a negative C isotope signature with $\delta^{13}C$ values rising up to 0‰ in the top. The second megacycle is

characterized by positive $\delta^{13}C$ values (up to 14‰), as usually found in post-Sturtian successions. The isotopic signature and facies analyses allow us to identify the FA2 deposits as a true post-glacial cap carbonate. This fact and the very high positive $\delta^{13}C$ found in the studied succession, associated with Pb–Pb geochronological data, allow us to propose that the Sete Lagoas is a Sturtian carbonate sequence.

Compared to other carbonate platforms of similar age, the Sete Lagoas deposits show peculiar characteristics. They are not base truncated and they present the whole transgressive sequence with the maximum flooding surface coinciding with the transition from negative to positive C isotope values. This new framework should carry out further stratigraphic studies in the region.

Acknowledgments

References

[1] F.F. Alkmim, S. Marshak, M.A. Fonseca, Assembly West Gondwana in the Neoproterozoic: Clues from the São Francisco craton region, Brazil, Geolog, Boulder, Colorado 29 (4) (2001) 319–322.

[2] P.A. Allen, P.F. Hoffman, Extreme winds and waves in the aftermath of a Neoproterozoic glaciation, Nature 433 (2005) 123–127.

[3] P.A. Allen, J. Leather, M.D. Brasier, The Neoproterozoic Fiq glaciation and its aftermath, Huqf supergroup of Oman, Basin Res. 16 (2004) 507–534.

[4] C.J.S. Alvarenga, R.V. Santos, E.L. Dantas, C–O–Sr isotopic stratigraphy of cap carbonates overlying Marinoan-age glacial diamictites of the Paraguay Belt, Brazil, Precambrian Res. 131 (2004) 1–21.

[5] M. Babinski, A.J. Kaufman, First direct dating of a Neoproterozoic post-glacial cap carbonate, IVth South American Symposium on Isotope Geology, short papers, (2003), pp. 321–323.

[6] M. Babinski, W.R. Van Schmus, F. Chemale, Pb–Pb dating and Pb isotope geochemistry of Neoproterozoic carbonate rocks from the São Francisco basin, Brazil: implications for the mobility of Pb isotopes during tectonism and metamorphism, Chem. Geol. 160 (1999) 175–199.

[7] M.D. Brasier, G. Shields, V.N. Kuleshov, E.A. Zhegallo, Integrated chemo- and biostratigraphic calibration of early animal evolution: Neoproterozoic–Early Cambrian of Southwest Mongolia, Geol. Mag. 133 (1996) 445–485.

[8] H.K. Chang, K. Kawashita, F.F. Alkmim, M.Z. Moreira, Considerações sobre a estratigrafia isotópica do Bambuí. In II Simp sobre o Cráton do São Francisco, Salvador, Atas (1993) 195–196.

[9] R.J. Cheel, D.A. Leckie, Hummocky cross-stratification, in : V.P. Wright (Ed.), Planet. Sci., 23, 1993, 451–478.

[10] F. Chemale, F.F. Alkmim, I. Endo, Late Proterozoic tectonism in the interior of the São Francisco craton, in : R.H. Findlay, et al. (Eds.), Gondwana Eight Assembly, Evolution and Dispersal, Balkema, 1993, 29–42.

[11] D. Condon, S. Bowring, W. Wang, A. Yang, Y. Jin, U–Pb Ages from the Neoproterozoic Doushantuo Formation, China, Science 308 (5718) (2005) 95–98.

[12] U.G. Cordani, K. Sato, W. Teixeira, C. Tassinari, M.A. Basei, Crustal evolution of South America Platform, in : U.G. Cordani, E.J. Milani, A. Tomaz-Filho, A.D. Campos (Eds.), Tectonic Evolution of South America, Proc. 31st International Geological Congress, Rio de Janeiro, Brazil, (2000), pp. 19–40.

[13] M.L. Corkeron, A.D. George, Glacial incursion on a Neoproterozoic carbonate platform in the Kimberley region, Australia, Geol. Soc. Am. Bull. 113 (2001) 1121–1132.

[14] F.A. Corsetti, A.J. Kaufman, Using chemostratigraphy to correlate and calibrate unconformities in Neoproterozoic strata from the southern Great Basin of the United States, Int. Geol. Rev. 42 (2000) 516–533.

[15] F.A. Corsetti, A.J. Kaufman, Stratigraphic investigations of carbon isotope anomalies and Neoproterozoic ice ages in Death Valley, California, GSA Bull. 115 (8) (2003) 916–932.

[16] M.T. Costa, J.J.R. Branco, Introdução, in : M.T. Costa, J.J.R. Branco (Eds.), Roteiro para a excursão Belo Horizonte–Brasília, SBG, Congresso Brasileiro de Geologia 14, Belo Horizonte, Anais 15, (1961), pp. 1–119.

[17] A. Cozzi, J.P. Grotzinger, P.A. Allen, Evolution of a terminal Neoproterozoic carbonates ramp system (Buah Formation, Sultanate of Oman): Effects of basement palaeotopography, Geol. Soc. Am. Bull. 116 (2004) 1367–1384.

[18] M.S. D'Agrella-Filho, M. Babinski, R.I.F. Trindade, W.R. Van Schmus, M. Ernesto, Simultaneous remagnetization and U–Pb isotope resetting in Neoproterozoic carbonates of the São Francisco craton, Brazil, Precambrian Res. 99 (2000) 179–196.

[19] M.A. Dardenne, Síntese sobre a estratigrafia do Grupo Bambuí no Brasil Central, SBG, Congresso Brasileiro de Geologia 30, Recife, Anais 2 (1978) 597–610.

[20] L.A. Derry, A.J. Kaufman, S.B. Jacobsen, Sedimentary cycling and environmental change in the Late Proterozoic: Evidence from stable and radiogenic isotopes, Geochim. Cosmochim. Acta 56 (1992) 1317–1329.

[21] D.A.D. Evans, Stratigraphic, geochronological and paleomagnetic constraints upon the Neoproterozoic climatic paradox, Am. J. Sci. 300 (2000) 347–433.

[22] C.M. Fanning, P.K. Link, U–Pb SHRIMP ages of Neoproterozoic (Sturtian) glaciogenic Pocatello Formation, southeastern Idaho, Geology 32 (2004) 881–884.

[23] G.J.B. Germs, The Neoproterozoic of southwestern Africa, with emphasis on platform stratigraphy and paleontology, Precambrian Res. 73 (1995) 137–151.

[24] P. Gorjam, M.R. Walter, R. Swart, Global Neoproterozoic (Sturtian) post-glacial sulfide-sulfur isotope anomaly recognized in Namibia, J. Afr. Earth Sci. 36 (2003) 89–98.

[25] J.P. Grotzinger, N.P. James, Precambrian Carbonates: Evolution of Understanding, Sediment. Geol. 67 (2000) 3–17.

[26] G.P. Halverson, A.C. Maloof, P.F. Hofman, The Marinoan glaciation (Neoproterozoic) in Northeast Svalbard, Basin Res. 16 (2004) 297–324.

[27] G.P. Halverson, P.F. Hofman, A.C. Maloof, S.A. Bowring, A.H. Rice, D.P. Schrag, F. Dudas, Towards a composite carbon isotope record for the Neoproterozoic, Geol. Soc. Am. Bull. 117 (2005) 1181–1207.

[28] J.C. Harms, J.B. Southard, R.G. Walker, Structures and sequences in clastic rocks, Soc. Econ. Paleontol. Miner. 249 (1982) (Short course, 9).

[29] J.M. Hayes, H. Strauss, A.J. Kaufman, The abundance of ^{13}C in marine organic matter and isotopic fractionation in the global biogeochemical cycle of carbon during the past 800 Ma, Chem. Geol. 161 (1999) 103–126.

[30] J.A. Higgins, D.P. Schrag, The aftermath of snowball Earth, Geochem., Geophys., Geosyst. 4 (2003) (No. 1028).

[31] K.H. Hoffman, D.J. Condon, S.A. Bowring, J.L. Crowley, U–Pb zircon date from the Neoproterozoic Ghaub Formation, Namibia: Constraints on Marinoan glaciation, Geology 32 (2004) 817–820.

[32] P.F. Hoffman, D.P. Schrag, The Snowball Earth hypothesis: testing the limits of global change, Terra Nova 14 (2002) 129–155.

[33] P.F. Hoffman, A.J. Kaufman, G.P. Halverson, Comings and goings of global glaciations on a Neoproterozoic tropical platform in Namibia, GSA Today, 8, 1998, pp. 1–9.

[34] S.S. Iyer, M. Babinski, H.R. Krouse, F. Chemale Jr., Highly ^{13}C-enriched carbonate and organic matter in the Neoproterozoic sediments of the Bambuí Group, Brazil, Precambrian Res. 73 (1995) 271–282.

[35] S.B. Jacobsen, A.J. Kaufman, The Sr, C and O isotopic evolution of Neoproterozoic seawater, Chem. Geol. 161 (1) (1999) 37–57.

[36] N.P. James, G.M. Narbonne, T.K. Kyser, Late Neoproterozoic cap carbonates: Mackenzie Montains, northwestern Canada: precipitation and global glacial meltdown, Can. J. Earth Sci. 38 (2001) 1229–1262.

[37] G. Jiang, N. Christie-Blick, A.J. Kaufman, D.M. Banerjee, V. Rai, Carbonate platform growth and cyclicity at a terminal Proterozoic passive margin, Infra Krol Formation and Krol Group, Lesser Himalaya, India, Sedimentology 50 (2003) 921–952.

[38] J. Karfunkel, A. Hoppe, Late Proterozoic glaciation in central Brazil: synthesis and model, Palaeogeogr., Palaeoclimatol., Palaeoecol. 65 (1988) 1–21.

[39] A.J. Kaufman, A.H. Knoll, Neoproterozoic variations in the C-isotopic composition of seawater: stratigraphic and biogeochemical implications, Precambrian Res. 73 (1995) 27–49.

[40] A.J. Kaufman, J.M. Hayes, A.H. Knoll, G.J.B. Germs, Isotopic composition of carbonates and organic carbon from upper Proterozoic successions in Namibia: Stratigraphic variation and the effects of diagenesis and metamorphism, Precambrian Res. 49 (1991) 301–327.

[41] M.J. Kennedy, Stratigraphy, sedimentology, and isotopic geochemistry of Australian Neoproterozoic postglacial cap dolostones: Deglaciation, δ^{13}C excursions, and carbonate precipitation, J. Sediment. Res. 66 (1996) 1050–1064.

[42] M.J. Kennedy, B. Runnegar, A.R. Prave, K.H. Hoffman, M.A. Arthur, Two or four Neoproterozoic glaciations? Geology 26 (1998) 1059–1063.

[43] M.J. Kennedy, N. Christie-Blick, L.E. Sohl, Are Proterozoic cap carbonates and isotopic excursions a record of gas hydrate destabilization following Earth's coldest intervals? Geology 29 (2001) 443–446.

[44] H. Kimura, K. Azmy, M. Yamamuro, J. Zhi-Wen, J.V. Cizdziel, Integrated stratigraphy of the Upper Neoproterozoic succession in Yunnan Province of South China: Re-evaluation of global correlation and carbon cycle, Precambrian Res. 138 (2005) 1–36.

[45] L.R. Kump, M.A. Athur, M.E. Patzkowsky, M.T. Gibbs, D.S. Pinkus, P.M. Sheehan, A weathering hypothesis for glaciation at high atmospheric pCO_2 during the Late Ordovician, Paleogeogr. Paleoclimatol. Paleoecol. 152 (1999) 173–187.

[46] N.J. Lorentz, F.A. Corsetti, P.K. Link, Seafloor precipitates and C-isotopic stratigraphy from the Neoproterozoic Scout Mountain Member of the Pocatello Formation, Southeast Idaho: implications for Neoproterozoic Earth system behavior, Precambrian Res. 130 (2004) 57–70.

[47] N. Machado, C.M. Noce, O.A. Belo de Oliveira, E.A. Ladeira, Evoluçũ geológica do Quadrilátero Ferrífero no Archeano e Proterozóico Inferior, com base em geocronologia U–Pb, in : V Simp. Geol. Núcleo Minas Gerais and I Simp, Geol. Núcleo Brasília, Belo Horizonte, Anais, 1989, pp. 1–5.

[48] D.M. McKirdy, J.M. Burgess, N.M. Lemon, X. Yu, A.M. Cooper, V.A. Gostin, R.J.F. Jenkins, R.A. Both, A chemostratigraphic overview of the Late Cryogenian interglacial sequence in the Adelaide Fold-Thrust Belt, South Australia, Precambrian Res. 106 (2001) 149–186.

[49] S. Marshak, F.F. Alkmim, Proterozoic contraction/extension tectonics of the southern São Francisco region, Minas Gerais, Brazil, Tectonics 8 (1989) 555–571.

[50] M.A. Martins-Neto, A.C. Pedrosa-Soares, S.A.A. Lima, Tectono-sedimentary evolution of sedimentary basins from Late Paleoproterozoic to Late Neoproterozoic in the São Francisco craton and Araçuaí fold belt, eastern Brazil, Sediment. Geol. 141–142 (2001) 343–370.

[51] A. Misi, J. Veizer, Neoproterozoic carbonate sequences of the Una Group, Irecê basin, Brazil: chemostratigraphy, age and correlations, Precambrian Res. 89 (1998) 87–100.

[52] R.M. Mitchum, J.C. Van Wagoner, High-frequency sequences and their stacking pattern: sequence-stratigraphic evidence of high-frequency eustatic cycles, in : K.T. Biddle, W. Schlager (Eds.), The Record of Sea-Level Fluctuations, Sediment. Geol. 70, 1991, pp. 131–160.

[53] G.M. Narbonne, J.D. Aitken, Neoproterozoic of the Mackenzie Mountains, northwestern Canada, Precambrian Res. 73 (1995) 101–121.

[54] A.C.R. Nogueira, C. Riccomini, A.N. Sial, C.A.V. Moura, T.R. Fairchild, Soft-sediment deformation at the base of the Late Neoproterozoic Puga cap carbonate (southern Amazon craton, Brazil): Confirmation of rapid icehouse-greenhouse transition in snowball Earth, Geology 31 (2003) 613–616.

[55] A.C. Pedrosa-Soares, U.G. Cordani, A. Nutman, Constraining the age of Neoproterozoic glaciation in eastern Brazil: first U–Pb (SHRIMP) data of detrital zircons, Rev. Bras. Geo. 30 (2000) 58–61.

[56] T.M. Peryt, A. Hoppe, T. Bechstadt, J. Koster, C.J. Pierre, D.K. Richter, Late Proterozoic aragonitic cement crusts, Bambuí Group, Minas Gerais, Brazil, Sedimentology 37 (1990) 279–286.

[57] R.V. Santos, C.J.S. Alvarenga, M.A. Dardenne, A.N. Sial, V.P. Ferreira, Carbon and oxygen isotope profiles across Meso-Neoproterozoic limestones from central Brazil: Bambuí and Paranoá groups, Precambrian Res. 104 (2000) 107–122.

[58] G.A. Shields, M.D. Brasier, P. Stille, D. Dorjnamjaa, Factor contributing to high $\delta^{13}C$ values in the Cryogenian limestones of western Mongolia, Earth Planet, Sci. Lett. 196 (2002) 99–111.

[59] D.P. Schrag, R.A. Bener, P.F. Hoffman, G.P. Halverson, On the initiation of a snowball Earth: Geochemistry, Geophysics, and Geosystems 3 (2002) 1036, doi:10.1029/2001GC000219.

[60] D.Y. Sumner, Decimetre-thick encrustations of calcite and aragonite on the sea-floor and implications for Neoarchaean and Neoproterozoic ocean chemistry, in : W. Altermann, P.L. Corcoran (Eds.), Precambrian sedimentary environments: A modern approach to ancient depositional systems, Int. Assoc. Sedimentol., Spec. Publ. 33, 2002, pp. 107–120.

[61] R.I.F. Trindade, M. Macouin, J. Besse, Paleolatitude of glacial deposits and paleogeography of Neoproterozoic ice-ages, C. R. Geoscience 339 (2007).

[62] A. Uhlein, R.R. Trompette, C.J.S. Alvarenga, Neoproterozoic glacial and gravitational sedimentation on a continental rifted margin: The Jequitaí-Macaúbas sequence (Minas Gerais, Brazil), J. South Am. Earth Sci. 12 (1999) 435–451.

[63] M.R. Walter, J.J. Veevers, C.R. Calver, P. Gerjan, A.C. Hill, Dating the 840–544 Ma Neoproterozoic interval by isotopes of strontium, carbon, and sulfur in seawater, and some interpretative models, Precambrian Res. 100 (2000) 371–433.

[64] R. Zhou, R. Tucker, S. Xiao, Z. Peng, X. Yuan, Z. Chen, New constraints on the ages of Neoproterozoic glaciations in south China, Geology 32 (2004) 437–440.